^{19}F Apparent Diffusion Coefficient MRI of Inert Fluorinated Gases in Human Lungs

Iain K. Ball[1], Marcus J. Couch[1,2], Tao Li[1,2], Matthew S. Fox[1], Jordan A. Lovis[1,2], Ralph Hashoian[3], Shalyn L. Littlefield[1], Birubi Biman[4], and Mitchell S. Albert[1,2]
[1]Thunder Bay Regional Research Institute, Thunder Bay, Ontario, Canada, [2]Lakehead University, Thunder Bay, Ontario, Canada, [3]Clinical MR Solutions, Brookfield, Wisconsin, United States, [4]Thunder Bay Regional Health Sciences Centre, Thunder Bay, Ontario, Canada

Introduction: Hyperpolarized noble gas MRI using ^{3}He or ^{129}Xe has emerged as a powerful technique for detecting microstructural changes in the lungs by measuring the apparent diffusion coefficient (ADC) of inhaled gases. ADC has been previously measured in human lungs using hyperpolarized ^{3}He MRI, which shows a strong correlation with tissue destruction and emphysema (1). More recently, ADC has been measured in patients with chronic obstructive pulmonary disease (COPD) using hyperpolarized ^{129}Xe MRI (2). Although these are very exciting developments, hyperpolarized noble gas MRI is not widely used because it is a complicated and expensive technique that requires specialized hardware. A possible alternative to hyperpolarized noble gases as a probe for measuring ADC is the use of inert fluorinated gases (SF_6, C_2F_6, C_3F_8) as an inhaled signal source for ^{19}F MRI of the lungs. Density-weighted ^{19}F imaging of inert fluorinated gases was initially reported in rat lungs 14 years ago (3). These gases have the advantages of being nontoxic, abundant, inexpensive, and they do not need to be hyperpolarized prior to their use in lung MRI. ADC measurements using inert fluorinated gas MRI has been previously reported in sealed phantoms (4), in rat lungs (5), and also in excised human lungs (6). Recently, Soher *et al*. demonstrated the clinical potential of ^{19}F MRI of inert fluorinated gases by performing density-weighted lung imaging in a healthy human subject (7). To our knowledge, ^{19}F ADC measurements have not been previously reported from the lungs of human subjects breathing inert fluorinated gases. In the present study, a ^{19}F 3D ultra-short TE (UTE) ADC pulse sequence was optimized for imaging human lungs with inert fluorinated gases at 3T.

Methods: This study protocol was approved by the local research ethics board and by Health Canada. All subjects provided written and informed consent prior to their participation in this study. Digital pulse oximetry was used to measure oxygen saturation (S_pO_2) for all subjects during scanning sessions. Imaging was performed using a 3.0 T Philips Achieva scanner with a flexible wrap-around quadrature transmit/receive coil tuned to the ^{19}F resonant frequency (Clinical MR Solutions). The ^{19}F coil was actively proton blocked to allow for ^{1}H imaging while the subject was lying in the ^{19}F coil. ^{1}H images were used as reference scans for planning 3D ADC-weighted ^{19}F images. Immediately prior to imaging, a healthy male subject inhaled a 1 L mixture of 79% C_3F_8 (perfluoropropane [PFP]) and 21% O_2 from a Tedlar bag. During a 33 second breath-hold, two 3D UTE images were acquired: an ADC-weighted image (b-value = 1.33 s·cm^{-2}, diffusion time = 1 ms) followed by an image without diffusion weighting. Image acquisition parameters were the following: TR = 34 ms, TE = 2.2 ms, flip angle = 68°, 75% radial sampling density, in-plane FOV = 450 x 450 mm^2, matrix = 64 x 64, three slices, thickness = 50 mm and a bandwidth of 140.7 Hz/pixel. Trajectory delays were optimized in order to compensate for eddy currents and gradient delays.

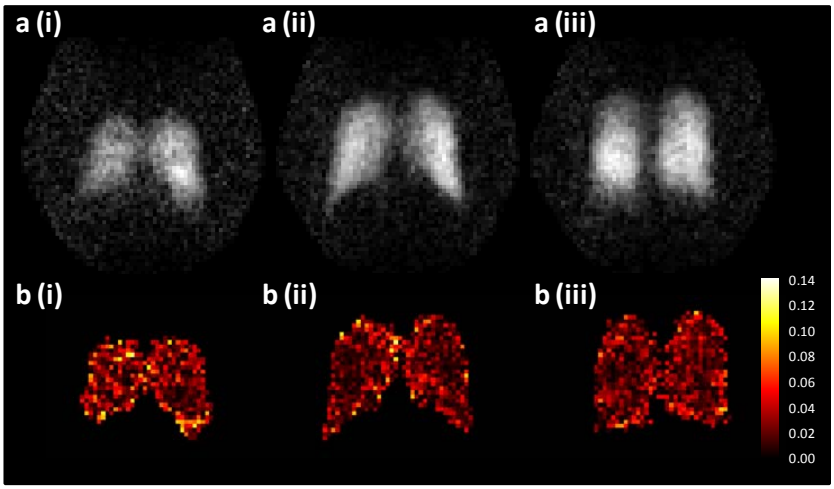

Figure 1: (a) ^{19}F 3D UTE lung images acquired in a healthy subject, and (b) the corresponding calculated ADC maps.

Results and Discussion: Figure 1(a) shows three slices from the ^{19}F 3D UTE image without diffusion weighting. The SNR in the center slice image was approximately 15. Figure 1(b) shows the ADC maps that were calculated from the images shown in Figure 1(a). Figure 2 shows the histograms corresponding to all three ADC maps shown in Figure 1(b). The mean ADC values were 0.034 ± 0.021 cm^2·s^{-1}, 0.023 ± 0.018 cm^2·s^{-1}, and 0.025 ± 0.017 cm^2·s^{-1} for Figures 2 (i), 2 (ii), and 2 (iii), respectively, where the error represents the heterogeneity in each respective ADC map. The ADC values reported in this study are similar to previously published values for the free diffusion of PFP (6). This is to be expected for a diffusion time of 1 ms and the subsequent diffusion length scale that was probed. A longer diffusion time will be required to reach the restricted diffusion regime that will allow quantitative measurement of surface to volume ratio, which is an important biomarker of lung microstructure. As noted with ^{129}Xe diffusion measurements, the lower diffusivity of ^{129}Xe, and other heavy gases such as PFP, compared to ^{3}He, may be one contributing factor leading to slower filling and lower diffusion in the terminal airways, possibly leading to larger disease-related defects (8). The subject's measured oxygen saturation never fell below 90%, and inhalation of the PFP/O_2 mixture was well tolerated. The use of a gas mixture containing 21% O_2 allows for continuous breathing; however, it should be noted that mixing PFP with other gases would increase the free diffusivity of PFP. In the future, ADC will be measured in patients with COPD using inert fluorinated gas MRI and compared to similar ADC measurements in healthy subjects.

Conclusion: This preliminary study effectively demonstrates the excellent potential of ^{19}F 3D UTE for measuring ADC in human lungs using inert fluorinated gases. This technique promises to provide valuable diagnostic information in the diagnosis and treatment of chronic respiratory diseases, such as COPD.

References:

[1] Evans A *et al*., (2008) *J Appl Physiol* 105:693–699.
[2] Kaushik SS *et al*., (2011) *Magn Reson Med* 65:1154–1165.
[3] Kuethe DO *et al*., (1998) *Magn Reson Med* 39:85–88.
[4] Chang YV *et al*., (2006) *J Magn Reson* 181:191–198.
[5] Perez-Sanchez JM *et al*., (2005) *Magn Reson Med* 54:460–463.
[6] Jacob RE *et al*., (2005) *Magn Reson Med* 54:577–585.
[7] Soher *et al*., (2010) *Proc. ISMRM*. p 3389.
[8] Kirby et al., (2012) Radiology 265:600–610.

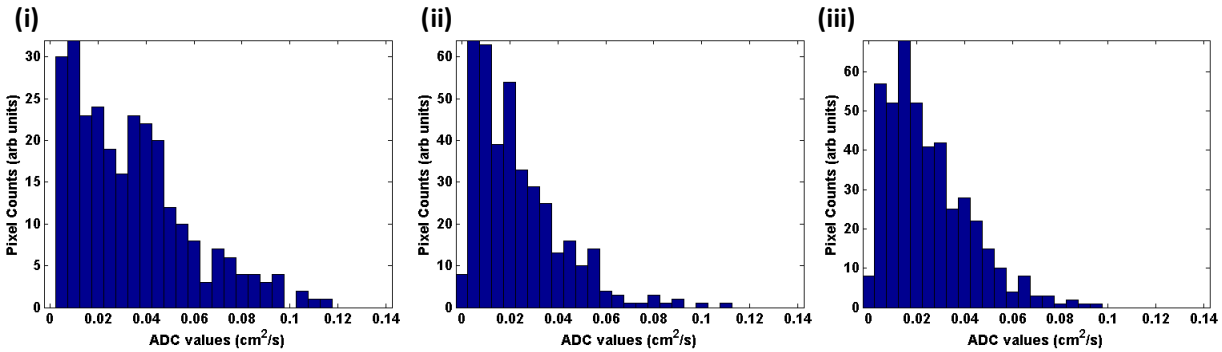

Figure 2: ^{19}F ADC histograms corresponding to the ADC maps shown in Figure 1(b).